Multi-scale study of Ti3SiC2 thin film growth mechanisms obtained by magnetron sputtering

C. Furgeaud, F. Brenet, J. Nicolai

Version of Record: https://www.sciencedirect.com/science/article/pii/S2589152919301656
Manuscript_de602a217cff8242a4668f2f5b8dea06

Multi-scale study of Ti_3SiC_2 thin film growth mechanisms obtained by magnetron sputtering

C. Furgeaud[a], F. Brenet[a], J. Nicolai[a,1,*]

[a]*Institut Pprime, UPR 3346, Université de Poitiers, SP2MI-Boulevard 3, Téléport 2-BP 30179, 86962 Futuroscope Chasseneuil Cedex, France*

Abstract

In the present work we focus on the mechanisms involved in Ti_3SiC_2 MAX phase thin-film formation and on the impact of stoichiometry and thickness/element quantity correlation. $TiAl_x$ thin-films, with $x = 0 - 2$, $100 - 300\,nm$ thick, were deposited by magnetron sputtering on a $SiC - 4H$ (0001) substrate. Samples were annealed at $1000°C$ for 30 minutes and analysed by XRD, AFM, SEM and TEM. The MAX phase Ti_3SiC_2 was formed at $1000°C$ in accordance with thermodynamic considerations. Moreover, an epitaxial relation between the film and the substrate occurred as follows $(0001)_{MAX}//(0001)_{SiC}$ and $[12\bar{1}0]_{MAX}//[12\bar{1}0]_{SiC}$ due to the formation of an earlier TiC phase by species interdiffusion. The catalytic role of Al has been demonstrated and explained by the formation of Ti_2AlC as precursor for Ti_3AlC_2 and for Ti_3SiC_2. Finally, second phases and continuity of films have been controlled by x and thickness factors. Indeed, the MAX phase film continuity is obtained for Al richer films, whereas the purest MAX phase have been synthesized for the thinnest layer of $TiAl_x$ deposited.

Keywords: MAX phase, thin films, epitaxy, TEM, magnetron sputtering

1. Introduction

$M_{n+1}AX_n$ phases ($n = 1-3$) consist in a large class of nanolaminated materials where M is an early transition metal element, A is an A-group element and X is either C or N [1, 2, 3, 4, 5, 6, 7]. For $n = 1, 2, 3$ the MAX phases are called 211, 312 and 413 respectively due to the periodic arrangement of their structure: M_6X octahedrons separated by A element layers in a hexagonal structure. This particular arrangement gives to the MAX phases a unique combination of metal and ceramic properties, opening the way to a large field of applications [8, 9, 10].

The Three Miles Island (1979, USA) and Fukushima Daiichi (2011, Japan) nuclear powerplant accidents demonstrated the importance to improve nuclear reactor safety. Thus, the concept of Accident Tolerant Fuel (ATF) has been introduced in order to improve the properties (oxidation, irradiation and corrosion resistance) of the Zircalloy full cladding during a cooling failure. In that way, some MAX phases are good candidates, indeed the Ti_3SiC_2 and Ti_2AlC MAX phases have been extensively studied due to their excellent properties, including irradiation resistance [11, 12, 13, 14, 15], oxidation resistance [16] and very specific mechanical properties [17]. The use of thin-film MAX-phase on SiC as cladding for nuclear fuel is one promising way. Moreover, Ti_3SiC_2 MAX phase thin-film on SiC can be used as ohmic contacts due to the very low contact resistance [18, 19, 20]. Several different techniques have been used to synthesize bulk MAX phases. Among these techniques, the most widespread is hot isostatic pressing (HIP) [5]; however, various techniques have been developed for the growth of MAX phase thin films using magnetron sputtering technology, either from elemental targets or from compound targets on various substrates [21, 22, 23, 24]. As shown on our recent papers, the co-deposition of Ti and Al on $SiC - 4H$ substrates leads, depending on annealing conditions, to the formation of either Ti_3SiC_2 or Ti_2AlC. Since mechanisms leading to each MAX phase remain a source of debate, it's difficult to predict product characteristics: MAX phase nature and microstructure [18, 25, 26]. The use of Al seems to be helpful to the synthesis of Ti_3SiC_2, although the mechanism is not well known [27, 20]. In the present study, we focus on the mechanisms involved in MAX phase formation at a high tem-

*Corresponding author
Email address: julien.nicolai@univ-poitiers.fr (J. Nicolai)

perature especially on the catalytic role of Al. We study the growth mechanisms of the Ti_3SiC_2 MAX phase depending on both, the stoichiometry and thickness of the fresh-deposited $TiAl_x$ layer. Ti_3SiC_2 formation was studied by XRD, AFM, SEM, STEM-HAADF, EDS and HRTEM in order to obtain relevant microstructure, chemistry and morphologies characterization, properties. The aluminium effect on the MAX phase thin film properties will be discussed by considering thermodynamic and kinetic effects.

2. Experimental Methods and Protocol

$SiC-4H$ substrates, single crystal (0001), n-type, supplied by TANKEBLUE, were used in this study. Al and Ti were co-deposited at room temperature onto SiC substrates by magnetron sputtering using pure Al (99.999%) and Ti (99.995%) targets in a high vacuum system (residual pressure $< 2.10^{-7}\,Pa$, Ar working pressure 0.3 Pa). Deposition parameters are summarized in table 1. Before deposition, the substrate was *in situ* cleaned by an etching at $60V$ during $600\,s$. Composition and thin film thickness have been checked using X-ray reflectometry (3000 Seifert) and SEM-EDS technique (JEOL 7001 TTLS) (Table 1).

Phases	Ti power (W DC)	Al power (W DC)	Working pressure (Pa)	Thickness (nm)
Ti	144	–	0.3	100
$TiAl$	300	158	0.3	100 / 300
$TiAl_2$	144	166	0.3	100 / 300

Table 1: Growth parameters used during magnetron sputtering deposition of all samples.

The samples were annealed in a vacuum lamp furnace (heating rate close to $20°C.s^{-1}$). Homogeneity of the samples (composition and thin film thickness) has been checked using X-ray reflectometry and SEM techniques. The structural investigations were performed by using X-Ray Diffraction (XRD) and Transmission Electron Microscopy (TEM). Diffraction experiments were conducted on a D8 Brucker AXS diffractometer operating in the Bragg-Brentano geometry under atmosphere environment. Diffractometer operates with a Cu tube and the K_β radiation is absorbed by a Ni filter in order to obtain a pure $Cu\ K_\alpha$ radiation ($\lambda = 0.15418\,nm$). The LynxEye detector is used for $\omega - 2\theta$ scans with a slight offset to avoid SiC reflections ($\omega - \theta = 0.2°$). Rocking curves have been achieved to investigate mosaicity of thin films with a classic scintillator detector. Conventional, High-Resolution TEM and Scanning Transmission Electron Microscopy (STEM) images were acquired using a JEOL 2200 FS (Schottky-FEG, $200\,kV$). The diffraction patterns and HRTEM micrographs were studied using JEMS software [28]. Using an Energy Dispersive x-ray Spectroscopy (EDS) detector (Bruker Quantax X flash 6) and an analytic single tilt-holder, Al, Ti and Si atomic composition were studied. Due to the carbon contamination induced by STEM, the carbon was detected but not quantified. TEM samples were prepared by Focus Ion Beam (FIB) using an FEI-HELIOS dual-beam using the lift-out classical method [29]. The surface morphology of the films was imaged after deposition and measured using a Nanoscope III Multimode Digital Instruments atomic force microscope (AFM) operating in tapping mode under air environment. All images were post-processed with WSxM software [30]. The surface roughness and lateral grain size were determined from Z-profile acquisitions. Surface analysis, topology and chemistry were achieved using SEM JEOL-7001F TTLS equipped with an EDS detector. SEM images were achieved at $5\,keV$ for $100\,nm$ sample thick and at $10\,keV$ for $300\,nm$ sample thick, while EDS analysis were acquired at $5keV$ considering L series of Ti and K series of Al, Si and C elements in order to limit bulk contribution.

3. Results

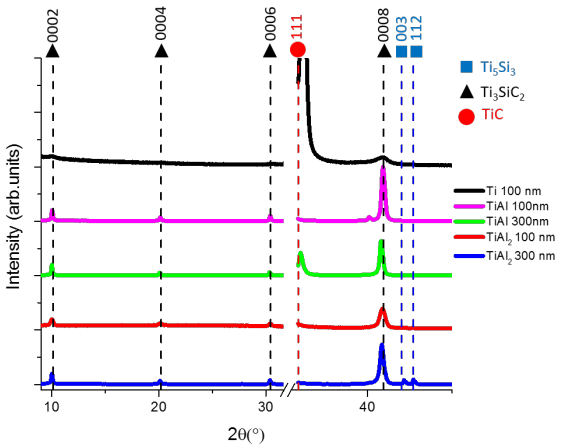

Figure 1: $\omega - 2\theta$ XRD diffractograms of Ti ($100\,nm$), $TiAl$ and $TiAl_2$ (both$100\,nm$ and $300\,nm$ thick) onto $4H-SiC$ annealed at $1000°C$ during $30\,min$. Black, blue and red dashed lines correspond to theoretical diffraction peak position for a pure Ti_3SiC_2 , Ti_5Si_3 and TiC powder respectively.

Fig.1 shows X-ray diffractograms of $TiAl - TiAl_2$, $100 - 300\,nm$ thick and $Ti - 100\,nm$ thick on SiC annealed at $1000°C$ for $30\,min$. Diffractogram of Ti deposited on SiC presents an intense peak at 35.9° attributed to (111) reflection of TiC structure. In order to obtain a more readable figure we show only the base of the peak allowing correct observations of other peaks present. Moreover, two weak peaks observed at 10.0° and 40.9° could be respectively attributed to (0002) and (0008) reflections of the Ti_3SiC_2 MAX phase. The four other diffractograms exhibit four peaks at 10.0°, 20.1°, 30.4° and 40.9° corresponding, respectively, to (0002), (0004),(0006) and (0008) reflections of the Ti_3SiC_2 MAX phase structure. Thus, all samples annealed, whatever thickness or stoichiometry, lead to formation of MAX phases. However, secondary peaks could be observed and are attributed to secondary phases. For $TiAl$ $100\,nm$, two very weak peaks are detected at 13.14° and 40.08°. These peaks could correspond to a slightly strained Ti_2AlC structure. Considering $TiAl$ $300\,nm$ the only secondary phase is TiC with the (111) reflection. In the case of $TiAl_2$, $300\,nm$, two reflections of Ti_5Si_3 are detected at 42.16° and 42.69° attributed to (300) and (112) planes respectively. Moreover the (111) reflection of $TiSi_2 - C54$ structure [31] is also observed at 27.74°. Finally, we can identify a broader peak for (0008) Ti_3SiC_2 reflection often explained by Al substitutions or interstitials. Moreover, the rocking curves achieved on the (0002) Ti_3SiC_2 peaks for all samples show a full width at half-maximum (FWHM) of 0.3° indicating a weak misorientation of the films as shown Fig.2 for the example case of $TiAl_2 - 300\,nm$.

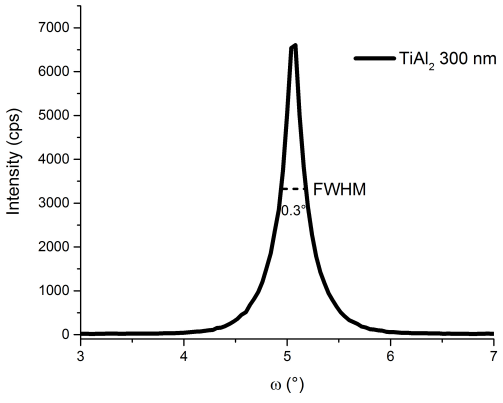

Figure 2: ω - scan at 2θ = 10.0° corresponding to the (0002) Ti_3SiC_2 peak. The full width at half maximum (FWHM) is 0.3° for the four samples.

Fig.3 shows the SEM micrographs of the top-viewed microstructure of samples after annealing at $1000°C$ during 30 minutes. EDS analyses reveal nude SiC areas without films on $100\,nm$ samples. Statistical study reveals a MAX phase covering rate close to 75% and 60% in the case of $TiAl$ $100\,nm$ and $300\,nm$ respectively, 95% and 100% in the case of $TiAl_2$ $100\,nm$ and $300\,nm$ respectively. Moreover, for the $TiAl_2$ samples SEM micrographs reveal grain boundary contrasts attesting to a polycrystalline film. Grains constituting films are faceted exhibiting hexagonal shape. More complex topography is observed on $TiAl$ sample without clear grain boundary contrasts. Discontinued films present many terraces on the surface but seem monocrystalline.

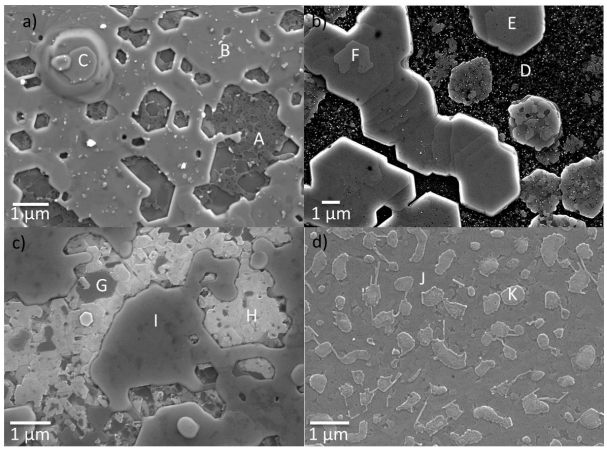

Figure 3: SEM micrographs of a) $TiAl - 100\,nm$, b) $300\,nm$, c) $TiAl_2 - 100\,nm$ and d) $300\,nm$ annealed $1000°C - 1x30min$. EDS analysed points are marked by letters from A to K.

Global and local EDS analyses have been achieved on these four samples and summarized in Table 2. As shown in this table the initial deposited ratio Ti/Al is not conserved. Indeed, the global Ti/Al ratio is much higher than ten, indicating a loss of aluminium during annealing. Local EDS analyses have been done on many areas in order to accumulate statistical data. We only show here average results per sample respectively named from A to K. As shown on Fig.3 and Table.2 the points A and G only probe SiC substrate. All the others points show the presence of Al, Ti, Si, and C elements.

As shown on Fig.4 the $TiAl$ samples exhibit some aggregates which are not present on the $TiAl_2$ samples. For the four specimens the RMS is close to $2\,nm$ for clean surfaces and close to $12\,nm$ for areas containing aggregates. The average height of terraces is close to $80\,nm$, $170\,nm$, $70\,nm$ and $70\,nm$ respectively measured

	$Al(\%)$	$Ti(\%)$	$Si(\%)$	$C(\%)$	$O(\%)$	Ti/Si ratio	Si/C ratio
TiAl 100 nm	**1**	**27**	**32**	**38**	**2**	**0.84**	**0.84**
A	0	0	50	50	0		
B	2	37	26	35	1	1.4	0.74
C	1	47	20	31	1	2.35	0.65
TiAl 300 nm	**1**	**17**	**37**	**44**	**1**	**0.45**	**0.84**
D	5	28	25	40	2	1.12	0.63
E	2	50	11	35	2	4.55	0.31
F	2	53	15	29	2	3.53	0.52
$TiAl_2$ **100 nm**	**0**	**18**	**40**	**41**	**0**	**0.45**	**0.98**
G	0	0	50	50	0		
H	1	29	29	40	1	1	0.73
I	1	42	20	37	0	2.1	0.54
$TiAl_2$ **300 nm**	**1**	**15**	**43**	**40**	**1**	**0.35**	**1.08**
J	1	44	22	32	1	2	0.69
K	3	55	33	9	3	1.83	3.33

Table 2: Local EDS results, bold letters correspond to the average composition of the entire sample and regular letters correspond to precise composition at the point letter.

on Fig.4a, 4b, 4c and 4d with a WsXM software plugin [30]. The highest point is respectively at 220 nm, 370 nm, 170 nm and 450 nm.

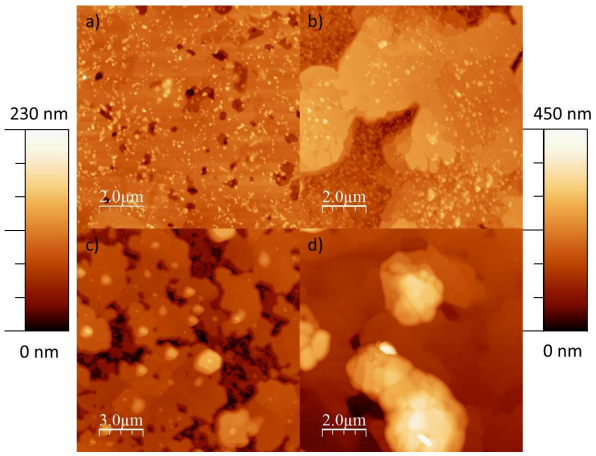

Figure 4: Surface morphology images of $TiAl$ a) 100 nm, b) 300 nm and $TiAl_2$ c) 100 nm, d) 300 nm annealed at $1000°C - 1x30min$.

Fig.5 shows the thin films obtained on $SiC - 4H$. The diffraction patterns obtained and the analysis of HRTEM micrographs show that the thin films correspond to 312 MAX phase structure. Moreover the MAX phase grows in epitaxy with $SiC-4H$ following the relation $(0001)_{MAX}//(0001)_{SiC}$ and $[12\bar{1}0]_{MAX}//[12\bar{1}0]_{SiC}$. The average thickness of the thin film is close to 130 nm, 220 nm, 50 nm and 100 nm for the samples A, B, C and D respectively. The film is very flat (Fig.6) and exhibits a very good crystallinity, however some areas without thin film on $SiC - 4H$ are also observed on samples A and C as expected from SEM images.

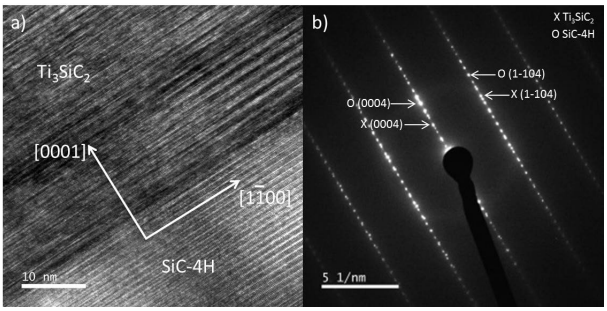

Figure 5: HRTEM micrograph of $TiAl - 100\,nm$ annealed $1000°C - 1x30min$ a) and associated diffraction pattern b). The diffraction pattern can be indexed using $SiC - 4H$ and Ti_3SiC_2 structures on $[11\bar{2}0]$ zone axis.

EDS analyses Fig.7, done on samples, show that the composition of the film is close to $75\%Ti$ for $25\%Si$ which corresponds to Ti_3SiC_2. Moreover, the Al presence at the interface between SiC and the Ti_3SiC_2 is observed for the samples B, C and D. The aluminium profile is spread over ten nanometers with a maximum value close to the SiC corresponding to 60%, 5% and 5% respectively for the samples B, C and D.

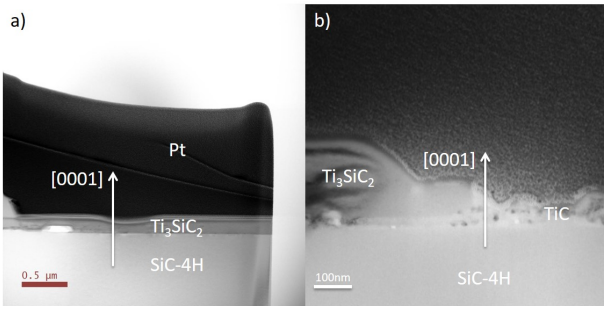

Figure 6: a) STEM micrograph of $TiAl_2 - 300\,nm$ annealed $1000°C - 1x30min$. b) BF-TEM micrograph of $TiAl - 300\,nm$ annealed $1000°C - 1x30min$.

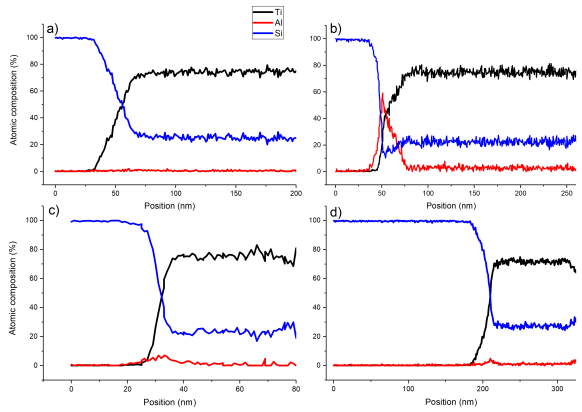

Figure 7: EDS line scan along growth direction for TiAl a) $100\,nm$, b) $300\,nm$ and $TiAl_2$ c) $100\,nm$, d) $300\,nm$ annealed at $1000°C - 1x30\,min$.

4. Discussion

4.1. Aluminium effect on Ti_3SiC_2 thin film formation

The results obtained on the $Ti - 100\,nm$ sample show that it is very difficult to form Ti_3SiC_2 using only Ti thin film even though all the elements are present. Moreover, the very intense peak of (111) TiC indicates that the Ti can easily interact with the SiC to form TiC by the following reaction:

$$SiC + Ti \rightarrow TiC + Si \tag{1}$$

as indicated by the negative free Gibbs energy $\Delta G^0 = -107\,kJ$ [32]. It seems that the formation of TiC structure in a silicon-rich environment is not enough to obtain Ti_3SiC_2 structure. As shown, the addition of Al strongly increases the amount of Ti_3SiC_2 obtained with the same annealing conditions. We assume that the role of aluminium in this mechanism is to obtain the 211 Ti_2AlC MAX phase by the following reaction:

$$2TiC + Al \rightarrow Ti_2AlC + C \tag{2}$$

Which is in a good agreement with DFT simulations [33]. Since the $Ti_{n+1}SiC_n$ system does not have the 211 phase, the silicon cannot be incorporated in the Ti_2AlC MAX phase [34]. We assume that the silicon will segregate above the Ti_2AlC. In a second time, the Ti_2AlC structure turns into a Ti_3AlC_2 structure. This reaction can be considered as a simple re-arrangement of the Ti_2AlC structure by releasing aluminium. At high temperature, it is well known that the 312 MAX phase is more stable than the equivalent 211 MAX phase [1]. Thus, the next step of the reaction is:

$$2Ti_2AlC \rightarrow Ti_3AlC_2 + (Ti, Al) \tag{3}$$

Once the Ti_3AlC_2 phase has been created, silicon above the Ti_3AlC_2 thin film diffuses through it, leading to substitution between Al and Si to form Ti_3SiC_2 MAX phase. The exchange of the A element of MAX phase has already been observed to form Ti_3AuC_2 starting from Ti_3SiC_2 [35]. By this way we assume that, in our conditions, the Ti_3SiC_2 structure is more stable than the Ti_3AlC_2 structure.

$$Ti_3AlC_2 + Si \rightarrow Ti_3SiC_2 + Al \tag{4}$$

The formation of the Ti_3SiC_2 structure is therefore highly enhanced by the Al presence due to the formation of 211 and 312 $Ti_{n+1}AlC_n$ MAX phases as summarized Fig.8.

4.2. Effect of aluminium stoichiometry on thin film growth mode

As shown by SEM and AFM on Fig.3 and Fig.4 the $TiAl_x$ stoichiometry has an important effect on the thin film growth mode. Indeed, for a defined thickness, the x-value of $TiAl_x$ tailors the surface morphology. In fact, for $x = 2$ the MAX phase layer appears continuous with terraces while for $x = 1$ some surfaces stay uncovered by the MAX phase. This observation might mean low Al concentration leading to higher surface diffusivity of both elements. Moreover, the uncovered areas have a different chemical composition depending on the thickness. Indeed, for the $100\,nm$ sample the uncovered areas consist in SiC while for the $300\,nm$ sample, they consist in TiC according to EDS-SEM and TEM analyses (Table 2 and Fig.6). A brief observation of the $Ti-Al$ phase diagram reveals that stoichiometry conditions to obtain $TiAl$ or $TiAl_2$ are a little bit different. Indeed, tolerance

of Al concentration to obtain $TiAl_2$ is less drastic than for $TiAl$ formation. In other words, in the case of Ti depletion for the $TiAl$ phase, the structure will be easily accommodated due to the large stoichiometry range of $TiAl$ stability in its diagram. However, the $TiAl_2$ phase is stable on a fine stoichiometry range of the diagram, thus depletion of Ti or Al could lead to phase changing subsequently leading to more complex diffusion mechanisms for Al and Ti. Thus, diffusion mechanisms of both elements and subsequent film growth morphologies depend on Al stoichiometry.

4.3. Effect of titanium quantity on MAX phase thickness

The main difference between $TiAl$ and $TiAl_2$ consists in the formation of secondary phases containing silicon or not. Moreover, the thickness of Ti_3SiC_2 thin film grown is higher for $TiAl$ than $TiAl_2$. In our magnetron sputtering chamber the amorphous deposited thin film has a density close to the theoretical one of the equivalent bulk crystal ($\rho_{TiAl_2} = 3.53\,g.cm^{-3}$ and $\rho_{TiAl} = 4\,g.cm^{-3}$). As such, for a similar thickness, $TiAl$ is two times titanium-rich than $TiAl_2$. For a similar $TiAl_x$ fresh-deposited film thickness, the synthesized MAX phase is thicker for $TiAl$ than $TiAl_2$. Considering AFM/SEM results and TEM observations we assume that the total quantity of MAX phase produced is higher for $TiAl$ than $TiAl_2$. As shown by TEM experiments the MAX phase layer is two times thicker for $TiAl$ than for $TiAl_2$ (Fig.7). Moreover, statistical studies achieved using SEM experiments showed that the MAX phase covering rate is higher than 50% for $TiAl$.

4.4. Effect of $TiAl_x$ thickness

$TiAl$ stoichiometry leads to a very pure Ti_3SiC_2 MAX phase for the $100\,nm$ sample and to Ti_3SiC_2 plus TiC for the $300\,nm$ sample. TEM observations, corresponding to a D region of Fig.3, have shown that the TiC has grown on SiC surface (Fig.6), which is in a good agreement with our assumptions about the first steps of MAX phase formation. Moreover, the presence of this phase could be explained by the lack of Al, not allowing the formation of Ti_2AlC and then the Ti_3SiC_2 phase.

$TiAl_2$ stoichiometry leads to the formation of a very pure and flat Ti_3SiC_2 MAX phase with a high coverage rate. For the $300\,nm$ sample we also observe secondary phases containing titanium and silicon like $TiSi_2 - C54$ or Ti_5Si_3 above the MAX phase corresponding to K region on the Fig.3.

The impact of thickness reagents has been already studied for a $Ti - Si - C$ system [36]. In this case the Al lack prevents the fast formation of MAX phase below $1\,\mu m$ of Ti. However, the increase of the thickness seems to help the increasing of Ti_3SiC_2 formation volume as observed on our systems.

4.5. Al presence after annealing

Surprisingly, only few traces of Al are detected on all samples by global and local SEM-EDS and by TEM/STEM -EDS techniques. Aluminium disappears from the bulk and the surface of thin films, indeed, it's not detected anymore either in MAX phases or in secondary products such as Ti_5Si_3 and $TiSi_2 - C54$. However, a poor quantity of aluminium was detected at the interface for three different samples: $TiAl$-$300\,nm$, $TiAl_2$-100 and $300\,nm$. The aluminium and silicon diffusion mechanisms toward a MAX phase Ti_3SiC_2 is the last step of our model. We assume that this process occurs from the surface to the interface. Thus, if the diffusion length is too long and the annealing time too short, it's not possible for all the aluminum sites to be substituted by silicon atoms. In this case, a very low quantity of Al is still trapped at the interface, not allowing formation of Ti_3SiC_2 but rather the conservation of Ti_3AlC_2. The conservation of this one could be considered as Al substitution and interstitial defects in the Ti_3SiC_2 MAX phase. Defects presence has been already suspected with XRD analysis with the broadening of the diffraction peak corresponding to (0008) plane of Ti_3SiC_2 for the sample $TiAl_2 - 300\,nm$ (Fig. 1).

In the case of $TiAl - 100\,nm$ we can admit that the thickness of the MAX phase is thin enough for silicon and aluminum co-diffusion, moreover, many lateral free surfaces exist (as shown on SEM image Fig. 3) creating more diffusion pathways. For the other three cases the MAX phase is thick enough to trap Al at the interface ($h_f = 200\,nm$ for $TiAl_x$-$300\,nm$) or not possess free lateral surfaces due to the continuity of the film ($TiAl_2$-$100\,nm$).

Moreover, we noticed at each annealing that the crucible containing the sample was covered with aluminium, indicating that the aluminium was coming out of the sample.

5. Conclusions

In the present work a two-step method to obtain epitaxial Ti_3SiC_2 thin film onto $SiC - 4H$ using magnetron sputtering deposition of $TiAl_x$ was studied for $x = 0$, 1 and 2. It was demonstrated that the addition of Al strongly increases the amount of Ti_3SiC_2 obtained by the formation of Ti_2AlC as a precursor for Ti_3SiC_2.

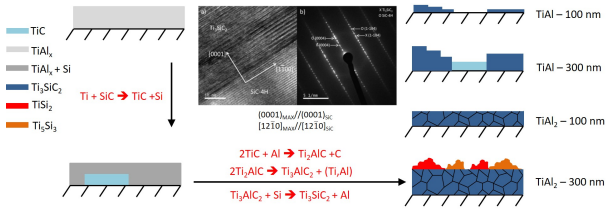

Figure 8: Schematic representation of Ti_3SiC_2 MAX phase thin-film formation.

Moreover, increase the amount of aluminum modifies the growth of Ti_3SiC_2 thin film and subsequent surface morphology from a discontinuous to a continuous layer. For $x = 1$ discontinuous films are monocrystalline and a lot of terraces emerge at the surface while $x = 2$ stoichiometry leads to continuous and polycrystalline films. Finally, the formation of secondary phases was observed for the $300\,nm$ samples, especially TiC for $x = 1$ and $TiSi_2 - C54$ plus Ti_5Si_3 for $x = 2$.

It seems that the stoichiometry is not the only relevant parameter: thickness seems to play a major role in MAX phase formation. The interdependence between stoichiometry and thickness on the Ti and Al quantity makes it possible to tailor the morphology, thickness and microstructure of the final MAX phase films. Moreover, the adjustment of these two interdependent parameters will be necessary in order to avoid secondary phase formation and obtain a pure and high quality MAX phase.

6. Aknowledgements

The authors would like to acknowledge P. Guerin for his technical support concerning magnetron sputtering and H. Bahsoun for the preparation of the TEM samples. The authors would like to specially thank E. Chasson for his help. This work partially pertains to the French Government program "Investissements d'Avenir" (LABEX INTERACTIFS, reference ANR-11-LABX-0017-01). This work has been partially supported by " Nouvelle Aquitaine " Region and by European Structural and Investment Funds (ERDF reference: P-2016-BAFE-94/95).

[1] P. Eklund, M. Beckers, U. Jansson, H. Högberg, L. Hultman, The Mn + 1AXnphases: Materials science and thin-film processing, Thin Solid Films 518 (8) (2010) 1851–1878. doi:10.1016/j.tsf.2009.07.184.

[2] M. Barsoum, MAX Phases: Properties of Machinable Ternary Carbides and Nitrides, wiley & so Edition, 2013.

[3] M. W. Barsoum, The MN+1AXN Phases: A New Class of Solids 28 (2000) 201–281. doi:10.1016/S0079-6786(00)00006-6.

[4] Z. M. Sun, Progress in research and development on MAX phases: a family of layered ternary compounds, International Materials Reviews 56 (3) (2011) 143–166. doi:10.1179/1743280410Y.0000000001.

[5] T. Lapauw, K. Lambrinou, T. Cabioc'h, J. Halim, J. Lu, A. Pesach, O. Rivin, O. Ozeri, E. N. Caspi, L. Hultman, P. Eklund, J. Rosén, M. W. Barsoum, J. Vleugels, Synthesis of the new MAX phase Zr2AlC, Journal of the European Ceramic Society 36 (8) (2016) 1847–1853. doi:10.1016/j.jeurceramsoc.2016.02.044.

[6] T. Lapauw, J. Halim, J. Lu, T. Cabioc'h, L. Hultman, M. Barsoum, K. Lambrinou, J. Vleugels, Synthesis of the novel Zr3AlC2 MAX phase, Journal of the European Ceramic Society 36 (3) (2016) 943–947. doi:10.1016/j.jeurceramsoc.2015.10.011.

[7] J. Gonzalez-Julian, J. Llorente, M. Bram, M. Belmonte, O. Guillon, Novel Cr2AlC MAX-phase/SiC fiber composites: Synthesis, processing and tribological response, Journal of the European Ceramic Societydoi:10.1016/j.jeurceramsoc.2016.09.029.

[8] M. W. Barsoum, M. Radovic, Elastic and Mechanical Properties of the MAX Phases, Annual Review of Materials Research 41 (1) (2011) 195–227. doi:10.1146/annurev-matsci-062910-100448.

[9] K. R. Whittle, M. G. Blackford, R. D. Aughterson, S. Moricca, G. R. Lumpkin, D. P. Riley, N. J. Zaluzec, Radiation tolerance of Mn+1AXn phases, Ti3AlC2 and Ti3SiC2, Acta Materialia 58 (13) (2010) 4362–4368. doi:10.1016/j.actamat.2010.04.029.

[10] T. Lapauw, A. K. Swarnakar, B. Tunca, K. Lambrinou, J. Vleugels, Nanolaminated ternary carbide (MAX phase) materials for high temperature applications, International Journal of Refractory Metals and Hard Materials 72 (2018) 51–55. doi:10.1016/j.ijrmhm.2017.11.038.

[11] C. Wang, T. Yang, S. Kong, J. Xiao, J. Xue, Q. Wang, C. Hu, Q. Huang, Y. Wang, Effects of He irradiation on Ti3AlC2: Damage evolution and behavior of He bubbles, Journal of Nuclear Materials 440 (1-3) (2013) 606–611. doi:10.1016/j.jnucmat.2013.04.070.

[12] M. K. Patel, D. J. Tallman, J. A. Valdez, J. Aguiar, O. Anderoglu, M. Tang, J. Griggs, E. Fu, Y. Wang, M. W. Barsoum, Effect of helium irradiation on Ti3AlC2 at 500C, Scripta Materialia 77 (2014) 1–4. doi:10.1016/j.scriptamat.2013.12.010.

[13] T. Yang, C. Wang, C. A. Taylor, X. Huang, Q. Huang, F. Li, L. Shen, X. Zhou, J. Xue, S. Yan, Y. Wang, The structural transitions of Ti3AlC2induced by ion irradiation, Acta Materialia 65 (2014) 351–359. doi:10.1016/j.actamat.2013.11.002.

[14] H. Zhang, R. Su, L. Shi, D. J. O'Connor, B. V. King, E. H. Kisi, The damage evolution of He irradiation on Ti3SiC2as a function of annealing temperature, Journal of the European Ceramic Society 38 (4) (2018) 1253–1264. doi:10.1016/j.jeurceramsoc.2017.11.041.

[15] H. H. Shen, F. Z. Li, H. B. Zhang, S. M. Peng, X. T. Zu, K. Sun, Effects of Xe+irradiation on Ti3SiC2at RT and 500C, Journal of the European Ceramic Society 37 (2) (2017) 855–858. doi:10.1016/j.jeurceramsoc.2016.08.026.

[16] Z. Sun, Y. Zhou, M. Li, High temperature oxidation behavior of Ti3SiC2-based material in air, Acta Materialia 49 (20) (2001) 4347–4353. doi:10.1016/S1359-6454(01)00247-6.

[17] M. Higashi, S. Momono, K. Kishida, N. L. Okamoto, H. Inui, Anisotropic plastic deformation of single crystals of the MAX phase compound Ti3SiC2 investigated by micropillar compression, Acta Materialia 161 (2018) 161–170. doi:10.1016/j.actamat.2018.09.024.

[18] A. Drevin-Bazin, J. F. Barbot, M. Alkazaz, T. Cabioch, M. F. Beaufort, Epitaxial growth of Ti3SiC2 thin films with basal planes parallel or orthogonal to the surface on α-SiC, Applied Physics Letters 101 (2) (2012) 2–5. doi:10.1063/1.4737018.

[19] A. Drevin-Bazin, J. F. Barbot, T. Cabioch, M. F. Beaufort, Investigation of Ti₃SiC₂ MAX Phase Formation onto N-Type 4H-SiC, Materials Science Forum 717-720 (2012) 845–848. doi:10.4028/www.scientific.net/MSF.717-720.845.

[20] S. Tsukimoto, K. Ito, Z. Wang, M. Saito, Y. Ikuhara, M. Murakami, Growth and Microstructure of Epitaxial Ti3SiC2 Contact Layers on SiC, Materials Transactions 50 (5) (2009) 1071–1075. doi:10.2320/matertrans.MC200831.

[21] R. Su, H. Zhang, D. J. O'Connor, L. Shi, X. Meng, H. Zhang, Deposition and characterization of Ti2AlC MAX phase and Ti3AlC thin films by magnetron sputtering, Materials Letters 179 (2016) 194–197. doi:10.1016/j.matlet.2016.05.086.

[22] R. Grieseler, B. Hähnlein, M. Stubenrauch, T. Kups, M. Wilke, M. Hopfeld, J. Pezoldt, P. Schaaf, Nanostructured plasma etched, magnetron sputtered nanolaminar Cr 2AlC MAX phase thin films, Applied Surface Science 292 (2014) 997–1001. doi:10.1016/j.apsusc.2013.12.099.

[23] Z. Feng, P. Ke, A. Wang, Preparation of Ti2AlC MAX Phase Coating by DC Magnetron Sputtering Deposition and Vacuum Heat Treatment, Journal of Materials Science and Technology 31 (12) (2015) 1193–1197. doi:10.1016/j.jmst.2015.10.014.

[24] R. Shu, F. Ge, F. Meng, P. Li, J. Wang, Q. Huang, P. Eklund, F. Huang, One-step synthesis of polycrystalline V2AlC thin films on amorphous substrates by magnetron co-sputtering, Vacuum 146 (2017) 106–110. doi:10.1016/j.vacuum.2017.08.049.

[25] A. Drevin-bazin, Module de puissance à base SiC fonctionnant à haute température Aspect matériaux.

[26] J. Nicolaï, C. Furgeaud, B. Fonrose, C. Bail, M. Beaufort, Formation mechanisms of Ti2AlC MAX phase on SiC-4H using magnetron sputtering and post-annealing, Materials & Design (2017). doi:10.1016/j.matdes.2018.02.046.

[27] T. Abi-Tannous, M. Soueidan, G. Ferro, M. Lazar, B. Toury, M. F. Beaufort, J. F. Barbot, J. Penuelas, D. Planson, Parametric investigation of the formation of epitaxial Ti3SiC2 on 4H-SiC from Al-Ti annealing, Applied Surface Science 347 (2015) 186–192. doi:10.1016/j.apsusc.2015.04.077.

[28] P. A. Stadelmann, EMS - a software package for electron diffraction analysis and HREM image simulation in materials science, Ultramicroscopy 21:131 (1987) 146.

[29] R. M. Langford, C. Clinton, In situ lift-out using a FIB-SEM system, Micron 35 (7) (2004) 607–611. doi:10.1016/j.micron.2004.03.002.

[30] I. Horcas, R. Fernández, J. M. Gómez-Rodríguez, J. Colchero, J. Gómez-Herrero, A. M. Baro, WSXM: A software for scanning probe microscopy and a tool for nanotechnology, Review of Scientific Instruments 78 (1). doi:10.1063/1.2432410.

[31] H. Inui, T. Hashimoto, K. Tanaka, I. Tanaka, T. Mizoguchi, H. Adachi, M. Yamaguchi, Defect and electronic structures in TiSi2 thin films produced by co-sputtering. Part 1: Defect analysis by transmission electron microscopy, Acta Materialia 49 (1) (2001) 83–92. doi:10.1016/S1359-6454(00)00296-2.

[32] I. Gotman, E. Y. Gutmanas, P. Mogilevsky, Interaction between SiC and Ti powder, Journal of Materials Research 8 (10) (1993) 2725–2733. doi:10.1557/JMR.1993.2725.

[33] J. Ward, S. Middleburgh, M. Topping, A. Garner, D. Stewart, M. W. Barsoum, M. Preuss, P. Frankel, Crystallographic evolution of MAX phases in proton irradiating environments, Journal of Nuclear Materials 502 (2018) 220–227. doi:10.1016/j.jnucmat.2018.02.008.

[34] V. J. Keast, S. Harris, D. K. Smith, Prediction of the stability of the Mn+1AXn phases from first principles, Physical Review B 80 (21) (2009) 214113. doi:10.1103/PhysRevB.80.214113.

[35] H. Fashandi, M. Dahlqvist, J. Lu, J. Palisaitis, S. I. Simak, I. A. Abrikosov, J. Rosen, L. Hultman, M. Andersson, A. Lloyd Spetz, P. Eklund, Synthesis of Ti3AuC2, Ti3Au2C2 and Ti3IrC2 by noble metal substitution reaction in Ti3SiC2 for high-temperature-stable Ohmic contacts to SiC, Nature Materials 16 (8) (2017) 814–818. doi:10.1038/nmat4896.

[36] H. Yang, X. Zhou, W. Shi, J. Wang, P. Li, F. Chen, Q. Deng, J. Lee, Y. H. Han, F. Huang, L. He, S. Du, Q. Huang, Thickness-dependent phase evolution and bonding strength of SiC ceramics joints with active Ti interlayer, Journal of the European Ceramic Society 37 (4) (2017) 1233–1241. doi:10.1016/j.jeurceramsoc.2016.12.009.